Modelling of heat flux received by a bubble pump of absorption-diffusion refrigeration cycles

Ali Benhmidene[1*], Béchir Chaouachi[1], Slimane Gabsi[1], Mahmoud Bourouis[2]

[1] Research Unit Environment, Catalysis and Process Analysis URECAP. The National School of Engineering of Gabès, Omar Ibn El Khattab Street, Gabes 6029, Tunisia

[2]Department of Mechanical Engineering, Universitat Rovira i Virgili, Av. dels Països Catalans, 26, 43007 Tarragona, Spain

(*) Corresponding author

Email: aahmiden@yahoo.fr

Telephone: +216 98642512

Abstract

In the present study, the heat flux received by a bubble pump, which was simulated to a vertical tube 1m long and with a variable diameter, was optimized. A numerical study was carried out in order to solve balance equations concerning the water-ammonia mixture in the up flow. The two-fluid model was used to derive the equations.

A numerical study was carried out on a heat flux between 1 and 70 $kW.m^{-2}$ and the liquid velocity was determined. The optimum flux was determined for a tube diameter equal to 4, 6, 8 and 10 mm and a mass flow rate ranging from 10 to 90 $kg.m^{-2}.s^{-1}$.

The optimum heat flux was correlated as a function of the tube diameter and mass flow rate, while the minimum heat flux required for pumping was correlated as a function of the tube diameter.

1 Introduction

The diffusion-absorption machine relies on a bubble pump to circulate the solution from the absorber to the boiler. A bubble pump is a fluid pump that operates on thermal energy to pump liquid from a lower level to a higher level. Many authors studied the influence of heat input and tube diameter on the performance of the bubble pump. Bourseau et al. [1] simulated a solar-driven bubble pump and reported the mass flow rates at various operating conditions. Stenning and Martin's model [2] was the starting point for Delano's [3] analysis of the bubble pump. It used an analytical model to investigate the influence of heat input, tube diameter and submergence ratio (the ratio between the liquid levels in the feeding tank and the liquid-vapor separator) on bubble pumps. Delano concluded that increasing the heat input to the bubble pump for a fixed submergence ratio increases the flow rate of the liquid through the bubble pump to a maximum and any further increase in the heat input decreases the liquid flow rate.

Pfaff et al. [4] studied the bubble pump with a lithium bromide–water vapor absorption cycle. They developed a mathematical model using the manometer principle to evaluate the bubble pump performance. They found that the pumping ratio is independent of the heat input. However, the frequency of the pumping action increases as the heat input to the bubble pump increases, or if the tube diameter decreases. The model was then used to analyze an ammonia-water system and it was found that the diameter that maximizes the efficiency of the bubble pump is between 4 mm and 26 mm for a liquid pumping rate between 0.0025 $kg.s^{-1}$ and 0.02 $kg.s^{-1}$. However, the efficiency rapidly decreases when diameters below the optimum values are used; therefore it is recommended that the diameter should be slightly larger than the optimum value.

Recently, Jakob et al. [5] reported that the indirectly heated generator with its bubble pump is the main new feature of a solar heat driven ammonia-water diffusion-absorption cooling machine and that all the prototypes constructed performed well. The performance of three diffusion absorption refrigeration (DAR) systems, which differ in their generator and bubble pump configuration, was studied numerically by Zohar et al. [6]. They showed that the configuration that integrated both the generator and the bubble pump is of great interest.

For all models, Stenning and Martin's theoretical method [2] is used as the starting point to set-up the relationship between the submergence ratio and the velocities (through momentum and mass balances). Additionally, each model (except for Delano's) uses Beattie and Whalley's model [7] to find the two-phase friction factor, and the drift flux model [8] to determine the gas void fraction. The difference between these two models is the value of the coefficients used in the drift flux model [9]. In all the studies mentioned above, heat is supplied at the bottom of the tube at a rate that is sufficient to boil some of the liquid.

In the present study, the bubble pump was a vertical uniformly heated tube with an ammonia-water mixture (40% of ammonia) operating at high pressure (P = 18 bar). This pressure is that of the condenser cooled with water at a temperature of 35°C. A numerical study based on two-fluid models was carried out to investigate the optimum heat flux input in the bubble pump. The effects of tube diameter and mass flux on the optimal heat flux were evaluated.

2 Mathematical modeling

The diffusion-absorption refrigeration cycle consists of a generator bubble pump, an absorber, an evaporator and a condenser, and usually operates with ammonia/water/hydrogen or helium as working fluid. Fig. 1 shows the main components of an absorption-diffusion refrigeration cycle and flow configurations in the bubble pump [10].

In the diffusion-absorption cycle, the bubble pump is a heated tube that lifts fluid from a lower reservoir to a higher one (Fig. 1). The generator configuration is of great importance. Heat is usually supplied at the bottom of the tube [4, 9, 11, and 12]. In the present work, heat is applied along all the tube length. This configuration of the bubble pump has two advantageous. First, it increases the coefficient of performance of the cycle (COP) using minimum heat as possible and desorbing as much refrigerant as possible [6]. Second, it can be heated using solar thermal energy by integrating the bubble pump tubes and the solar collector [13-15].

In the present work, the two-fluid model was used for the two-phase flow region considering the hydrodynamic and thermodynamic non-equilibrium between the liquid and vapor phases. The flow configuration was not limited to the slug regime [3, 4, 9], starting as bubbly and ending as annular (Fig.1). The mathematical model used is described below.

Heating causes the onset of boiling somewhere downstream of the pump entrance. In the two-phase region, the general conservation equations of mass, momentum and energy were formulated by Ishii and Mishima [16]. In steady-state regime with negligible kinetic and potential energy, the conservation equations can be reduced to the following five equations:

- Phase mass equations

$$\frac{\partial}{\partial z}\left(\alpha\rho_G u_G\right)=\Gamma_G \tag{1}$$

$$\frac{\partial}{\partial z}\left[\left(1-\alpha\right)\rho_L u_L\right]=\Gamma_L \tag{2}$$

- Phase momentum equations

$$\frac{\partial}{\partial z}\left(\alpha\rho_G u_G^2\right)+\alpha\frac{\partial P}{\partial z}+\alpha\rho_G g=-F_{WG}-F_{GL}-F_{GI} \tag{3}$$

$$\frac{\partial}{\partial z}\left[\left(1-\alpha\right)\rho_L u^2{}_L\right]+\left(1-\alpha\right)\frac{\partial P}{\partial z}+\left(1-\alpha\right)\rho_L g=-F_{WL}+F_{LG}-F_{LI} \tag{4}$$

- Mixture energy equation

$$\frac{\partial}{\partial z}\left[(1-\alpha)\rho_L u_L H_L+\alpha\rho_G u_G H_G\right]=\frac{q_w P_h}{A} \tag{5}$$

The drag force F_{LG} is modelled according to Richter [17]:

$$F_{LG}=\frac{3C_{FI}}{D}\sqrt{\alpha}\rho_G\left(u_G-u_L\right)\left|u_G-u_L\right|+C^{'}\rho_G u_G\alpha\frac{d}{dz}\left(u_G-u_L\right) \tag{6}$$

C' is a virtual mass transfer coefficient assumed to be 0.5 for bubbly flow and 0 for other flow regimes.

The interfacial friction factor C_{FI} is taken as [17]:

$$\begin{cases} C_{FI}=C_D\sqrt{\alpha}\left(1-\alpha\right)^{-1.7}\dfrac{\rho_L}{\rho_G}\dfrac{D}{D_B} \\ \text{for bubbly flow} \\ C_{FI}=0.005\left(1+75\left(1-\alpha\right)\right) \\ \text{for annular flow} \end{cases} \tag{7}$$

In the churn turbulent flow with medium void fraction between the bubbly and annular flow, C_{FI} is interpolated linearly with the void fraction between the two values given in Eq. (7).

The drag coefficient for a single bubble C_D in Eq. (7), which depends on the bubble Reynolds number Re_B, is modeled according to Wallis [18]:

$$C_D = \frac{24}{\mathrm{Re}_B}\left(1+0.15\,\mathrm{Re}_B^{0.687}\right) \qquad \mathrm{Re}_B < 1000 \tag{8}$$

$$C_D = 0.44 \quad \mathrm{Re}_B \geq 1000 \tag{9}$$

$$\text{Where } \mathrm{Re}_B = \frac{2\rho_L R_B (1-\alpha)\left|u_G - u_L\right|}{\mu_L} \tag{10}$$

The interfacial momentum transfers F_{GI} and F_{LI} caused by mass transfer, when the liquid is evaporated, can be determined from equations (3) and (4). The force associated with this velocity change is described by the following terms:

$$F_{LI} = -(1-\eta)\Gamma_L\left(u_L - u_G\right) \tag{11}$$

$$F_{GI} = -\eta\Gamma_G\left(u_G - u_L\right) \tag{12}$$

η is the phase distribution factor, η = 0.5 for bubbly flow regime and η = 0 for the other flow regimes [17].

The wall liquid friction F_{WL} is modelled by Chisholm's [19] correlation because it fits Baroczy's advanced empirical correlation curves [20] quite well and takes into account the effect of mass flux on the friction pressure gradient. The correlation is expressed by the following set of equations:

$$F_{WL} = \left[1+\left(Y^2-1\right)\left(Bx^{(2-n)/2}\left(1-x\right)^{(2-n)/2}+x^{2-n}\right)\right]\Delta P_{Lo} \tag{13}$$

Where ΔP_{Lo} is the single-phase friction pressure drop which would exist if the total mass flow of the two-phase mixture flowed as liquid phase only. It is given by:

$$\Delta P_{Lo} = \frac{4}{D} f_{Lo} \frac{G^2}{2\rho_L} \tag{14}$$

n = 0.25 for the Blasius equation.

$$Y = \left(\frac{\Delta P_{Go}}{\Delta P_{Lo}}\right)^{0.5} = \left(\frac{f_{Go}}{f_{Lo}}\right)^{0.5} \tag{15}$$

Coefficient B in equation (13) is denoted as [19]:

$$B = \frac{CY - 2^{2-n} + 2}{Y^2 - 1} \tag{16}$$

Where $C = \frac{u_G}{u_L}\sqrt{\frac{\rho_L}{\rho_G}}\left(1 + \frac{u_G^2}{u_L^2}\frac{\rho_G}{\rho_L}\right)$ [19] (17)

And the true vapour mass quality is expressed as:

$$x = \frac{1}{1 + \frac{1-\alpha}{\alpha}\frac{\rho_L}{\rho_G}\frac{U_L}{U_G}} \tag{18}$$

The vapour generation rate is given by the following expression:

$$\Gamma_G = -\Gamma_L = \frac{q_e}{h_{fg} + Cp_L.\Delta T_{sat}} \tag{19}$$

The heat transfer rate q_e due to evaporation can be modelled by the following equation:

$$q_e = C_2\left(q_w - C_1 h_{sp}\left(T_w - T_L\right)\right) \tag{20}$$

C_1 and C_2 were correlated by Hainoun et al. [21]:

$$C_1 = 1 - \frac{\pi}{16}\frac{\alpha}{\alpha_{OSV}} \; for \; \alpha \le \frac{16.\alpha_{OSV}}{\pi}$$
$$C_1 = 0 \; for \; \alpha \succ \frac{16.\alpha_{OSV}}{\pi} \tag{21}$$

$$C_2 = \left(\frac{T_w - T_{sat}}{T_w - T_L}\right)^2 \tag{22}$$

h_{sp} is the single liquid phase heat transfer coefficient given by:

$$h_{sp} = 0.023\frac{\lambda_L}{D}\mathrm{Re}_L^{0.8}\,\mathrm{Pr}_L^{0.4} \tag{23}$$

Re_L is the Reynolds number in the liquid phase expressed by:

$$\mathrm{Re}_L = \frac{GD(1-x)}{\mu_L} \tag{24}$$

The wall temperature T_w is calculated from:

$$q_w = h_{tp}\left(T_w - T_L\right) \tag{25}$$

The method for expressing the forced convection boiling heat transfer coefficient h_{tp} is derived from Chen's well-known correlation [22]. This method was used by Celata et al. [23] to predict the convective boiling heat transfer coefficient for R12/R114 binary mixtures.

3 Numerical solution

Equations (1-5), which govern the evaporation of refrigerant flowing in the vertical tube, have five unknown parameters: namely, α, u_L, u_G, P, and H_L. To solve this set of equations numerically, the tube was divided into infinitesimal sections. The heat flux, q_w, and the operating conditions shown in table 1 were considered.

The equations were solved using the fourth order Runge-Kutta method.

4 Model Validation

To validate the two-fluid model presented above a comparison of the calculated values for void fraction versus vapor quality using this model was compared with those obtained from three other models, that is:

- The homogenous model

$$\alpha = \frac{1}{1 + \frac{\rho_G}{\rho_L}\left(\frac{1-x}{x}\right)} \tag{26}$$

- The Rouhani and Axlesson drift model [24]

$$\alpha = \frac{x}{\rho_G}\left\{\left(1 + 0.12(1-x)\left(\frac{gDh\rho_L^{\,2}}{G_o^{\,2}}\right)^{0.25}\right)\left(\frac{x}{\rho_G} + \frac{1-x}{\rho_L}\right) + \frac{1.18}{G_o}\times\left[\frac{g\sigma(\rho_L - \rho_G)}{\rho_L^2}\right]^{0.25}(1-x)\right\}^{-1} \tag{27}$$

- The Zivi annular model [25].

$$\alpha = \frac{1}{1+\left(\frac{\rho_G}{\rho_L}\right)^{0.67}\left(\frac{1-x}{x}\right)} \quad (28)$$

Void fraction was calculated at the operating conditions reported in Table 1 and the heat flux and mass flux were set to constant values of 20 kW.m^{-2} and 50 kg.m^{-2}.s^{-1}, respectively.

It can be observed in Fig. 2 that the numerical values achieved in the present work show similar trend to the results of other models. For void fractions lower than 0.6 there is a great similarity between the calculated values using Rouhani and Axelsson's correlation and our results, being the absolute deviation between 1.3 and 8.0 %. For void fractions above 0.6, the absolute deviation is larger and can reach 17.0 %. Regarding the Zivi's model, which is applicable for annular flow regime (α> 0.8), it gives values very close to our simulation results. The absolute deviation of this model does not exceed 5.5% and may decrease to 0.37%. The difference deviation between the values from the homogenous model and our numerical results is significant. This is due to the fact that in the homogenous model it is assumed that both liquid and vapour phases are flowing with the same velocity, which is not the case in our model as well as in practice.

The good agreement between these results indicates that the two-fluid model is suitable for the prediction of refrigerant two-phase flow in bubble pumps.

5 Simulated results

5.1 Optimum heat flux

Solving the system of equations of the mathematical model, as well as the values of void fraction, temperature and pressure, made possible the determination of the weak solution and refrigerant velocities through the bubble pump tube.

The outlet velocity of the weak solution was determined for the values given in table 1 for heat flux, tube diameter, and mass flow rate. The liquid velocity was calculated once the steady-state regime was established (i.e. for a fixed mass flow rate; G). Fig.3 illustrates the evolution of the weak solution velocity versus heat flux for G = 50 $kg.m^{-2}.s^{-1}$. As it can be observed, for different tube diameters, the weak solution velocity increases with heat flux to a maximum value and then decreases.

The flow regime changes from bubbly flow, for which the velocity is at its low value, to slug flow, where it is at its maximum value. When the velocity decreases, churn flow appears (Fig. 1). Experimental studies [3-6, 8] showed that the bubble pump is more efficient when it operates in the slug flow regime. At fixed operating conditions and geometrical parameters the bubble pump generates optimum heat flux in slug flow regime at the highest liquid velocity. Fig. 3 shows that the optimum heat flux depends on the tube diameter of the bubble pump.

To model this dependency, optimum heat flux versus tube diameter is plotted in Fig. 4 at different mass flow rate values. This figure shows that the optimum heat flux depends on both tube diameter and mass flow rate. For a given mass flow rate, optimum heat flux is linearly related to tube diameter as follows:

$$q_{op} = a.D + b \tag{29}$$

Table 2 shows a and b values as well as the regression coefficient R^2. The parameters a and b depend on the mass flow rate. Fig. 5 shows the evolution of these parameters versus the mass flow rate G. Parameters a and b vary linearly with G and are given, respectively, by:

$$a = 68.75G + 828.5 \quad (30)$$

$$b = 30.8G - 2416 \quad (31)$$

The above results show that optimum heat flux depends on both tube diameter and mass flow rate according to equation (32):

$$q_{op} = (68.75G + 828.5)D + 30.8G - 2416 \quad (32)$$

5.2 Minimum heat flux required for pumping

In order to predict the minimum heat flux required for pumping the liquid through the bubble pump, the variation of the optimum heat flux versus mass flow rate at different diameters is plotted in Fig.6. This figure indicates that the optimum heat flux varies linearly with the mass flow rate when the tube diameter is kept constant.

Fig. 6 shows the existence of two special parameters a' and b', where a' denotes the slope of each line, and b' is the ordinate at the origin that corresponds to the heat flux just before the liquid starts circulating. The ordinate at origin b' is the minimum heat flux, denoted q_{min}, required for pumping, which depends on tube diameter (see Fig. 6). Fig. 7 illustrates that the minimum heat flux q_{min} varies linearly with the tube diameter D according to the following equation:

$$q_{min} = 878D - 2416 \quad (33)$$

6 Conclusions

The two-fluid model was used in a numerical study designed to optimize the heat flux required for optimal operation of a bubble pump considered to be a vertical tube of a given length and variable diameter. The working fluid considered was an ammonia-water mixture with 40% in ammonia by weight.

Solving numerically the governing equations of the system, the weak solution velocity through the tube was then calculated. By varying this velocity versus the supplied heat flux ranging from 1 kW.m^{-2} to 70 kW.m^{-2} the optimum heat flux was determined.

In this study, the optimum heat flux was correlated as a function of the tube diameter and mass flow rate as follows: $q_{op} = (68.75G + 828.5)D + 30.8G - 2416$.

Also, the minimum heat flux required for pumping was correlated as a function of the tube diameter according to: $q_{\min} = 878D - 2416$

Acknowledgements

This work is part of a R&D project funded by the Spanish Ministry of Science and Innovation within the Energy Program: ENE2006-15250.

Nomenclatures

A : tube cross-section area (m^2)

C_1 : the portion of the heating surface not covered by bubbles

C_2 : coefficient related to the pumping factor

C' : virtual mass coefficient

C_D : drag coefficient for a single bubble

C_{FI} : interfacial friction factor

C_P : specific heat (J.kg^{-1}.C^{-1})

D : hydraulic diameter (m)

f_{Lo} : fraction factor

F_{GI} : interfacial force for the vapor due to the mass exchange (N.m^{-3})

F_{LG} : interfacial force between the two phases (N.m^{-3})

F_{LI} : interfacial force for the liquid due to the mass exchange (N.m^{-3})

F_{WG} : force between the wall surface and the vapor ($N.m^{-3}$)

F_{WL} : force between the wall surface and the liquid ($N.m^{-3}$)

g : gravity acceleration ($m.s^{-2}$)

G : mass flow in the tube ($kg.m^{-2}.s^{-1}$)

H : enthalpy ($J.kg^{-1}$)

h : heat transfer coefficient ($Wm^{-2}.K^{-1}$)

h_{fg} : evaporation heat from the liquid to the vapor ($J.kg^{-1}$)

L : length (m)

P : pressure (Pa)

P_h : heating perimeter of the channel (m)

Pr : Prandtl number

q : total wall heat flux ($W.m^{-2}$)

R_B : bubble radius (m)

Re_B : bubble Reynolds number

T : temperature, K

u : velocity ($m.s^{-1}$)

x : vapour quality

Xtt : Lockhart-Martenelli parameter

z : axial location along the flow direction (m)

Greek symbols

α : void fraction

μ : dynamic viscosity (Pa.s)

ρ : density ($kg.m^{-3}$)

σ : surface tension ($N.m^{-1}$)

Γ : vapor or liquid generation rate per unit mixture volume ($kg.m^{-3}.s^{-1}$)

ΔP : pressure drop (Pa)

Index

L : liquid

Lo : liquid only

Go : vapor only

B : bubble

H : hydraulic

L : liquid

In : inlet

G : vapor

OSV : onset of significant void

sat : saturation condition

W : wall

CV : convective

tp : tow phase

References

[1] Bourseau P, Mora JC, Bugare R (1987) Coupling of an absorption-diffusion refrigeration machine and solar flat-plate collector. Int J Refrigeration 9:206-214

[2] Stenning AH, Martin CB (1968) An analytical and experimental study of air-lift pump performance. Transactions of the ASME Journal of Engineering for Power (April) 106-110.

[3] Delano AD (1998) Design analysis of the Einstein refrigeration cycle. Ph D Dissertation, Georgia Institute of Technology.

[4] Pfaff M, Saravanan R, Maiya MP, Srinivasa M (1998) Studies on bubble pump for a water–lithium bromide vapor absorption refrigeration. Int J Refrigeration 21:452–462.

[5] Jakob U, Eicker U, Schneider D, Taki AH, Cook, MJ (2008) Simulation and experimental investigation into diffusion absorption cooling machines for air-conditioning application. Appl Therm Eng 28:1138-1150.

[6] Zohar A, Jelinek M, Levy A, Borde I (2008) The influence of the generator and bubble pump configuration on the performance of diffusion absorption refrigeration (DAR) system. Int J Refrigeration 31: 962-969

[7] Beattie DRH, Whalley PB (1982) A simple two-phase frictional pressure drop calculation method. Int J Multiphase Flow 8:83-87.

[8] Zuber N, Findlay J (1965) Average volumetric concentration in two-phase flow Systems. J Heat Transfer 87: 453-468.

[9] White SJ 2001 Bubble pump design and performance. M.Sc Thesis, Georgia Institute of Technology.

[10] Platen BCV, Munters CG (1928) Refrigerator, U.S. Patent No 1: 685-764.

[11] Koyfman A, Jelinek M, Levy A, Borde I (2003) An experimental investigation of bubble pump performance for diffusion absorption refrigeration system with organic working fluids. App. Ther. Engineering, 23:1881–94.

[12] Vicatos G, Bennett A (2007) Multiple lift tube pumps boost refrigeration capacityin absorption plants. J. Energy S. Africa, 18: 49-57.

[13] Jakob U, Eicker U, Schneider D, Cook MJ, Taki AH (2008) Simulation and experimental investigation into diffusion absorption cooling machines for air-conditioning applications. App. Ther. Engineering, 28: 1138-1150.

[14] Chaouachi B, Gabsi S (2007) Design and Simulation of an Absorption Diffusion Solar Refrigeration Unit. Am. J. Applied Sciences, 4: 85-88.

[15] Gutierrez F (1988) Behavior of a household absorption diffusion refrigerator adapted to autonomous solar operation. Solar Energy, 40: 17-23.

[16] Ishii M, Mishima K (1984) Two-fluid model and hydrodynamic constitutive relations. Nucl Eng Design 82:107-126.

[17] Wallis GB (1969) One-dimensional Two-phase Flow. McGraw-Hill.

[18] Richter HJ (1983) Separated two-phase flow model: application to critical two phase flow. Int J Multiphase Flow 9:511-530.

[19] Chisholm D (1973) Pressure gradient due to friction during the flow of evaporating two phase mixtures in smooth tubes and channel. Int J Heat and Mass transfer 16:347358.

[20] Baroczy CJ (1965) A systematic correlation for two-phase pressure drop. Chem. Eng. Prog Simpson Series 62:232–249

[21] Hainoun A, Hicken E, Wolters J (1996) Modelling of void formation in the subcooled boiling regime in the ATHLET code to simulate flow instability for research reactors. Nucl Eng Design 16:7175-191

[22] Chen JC (1966) Correlation for boiling heat transfer to saturated fluids in convective flow. Ind Eng Chem Process Design and Development 5**:**322-329.

[23] Celeta GP, Cumo M, Satero T (1993) Forced convective boiling in binary mixtures. Int J Heat and Mass Transfer 36:3299-3309

[24] Rouhani Z, Axelsson E (1970) Calculation of volume void fraction in the subcooled and quality region. Int J Heat Mass Transfer 13:383–93.

[25] Zivi SM (1964) Estimation of steady state steam void fraction by means of principle of minimum entropy production. Trans. ASME. J. Heat Transfer 86: 247–252.

Table 1 Operating conditions considered for simulation

Parameter	Values
Heat flux ($kW.m^{-2}$)	1 - 70
Tube diameter (mm)	4 ; 6 ; 8 ; 10
Mass flow rate ($kg.m^{-2}.s^{-1}$)	10 ; 30 ; 50 ; 70 ; 90
Tube length (m)	1,000
Ammonia concentration at the inlet	0,4
Inlet pressure pump (bar)	18

Table 2 Values of parameters a, b and the regression coefficient R^2

Mass flow rate ($kg.m^{-2}.s^{-1}$)	a ($kW.m^{-3}$)	b ($kW.m^{-2}$)	R^2
10	1395	-2.09	0.9997
30	2890	-1.58	0.9987
50	4680	-0.81	0.9998
70	5600	-0.20	0.9974
90	6850	0.30	0.9962

Figure captions

Fig. 1 Main components of an absorption-diffusion refrigeration cycle and flow configurations in the bubble pump

Fig. 2 Comparison of void fraction simulated with other models

Fig. 3 Liquid velocity versus heat flux

Fig. 4 Optimum heat flux versus tube diameter for different mass flow rates G

Fig. 5 Variations of parameters a and b versus the mass flow rate G

Fig. 6 Optimum heat flux versus mass flow rate for different tube diameter values

Fig. 7 Variations of minimum heat versus tube diameter D

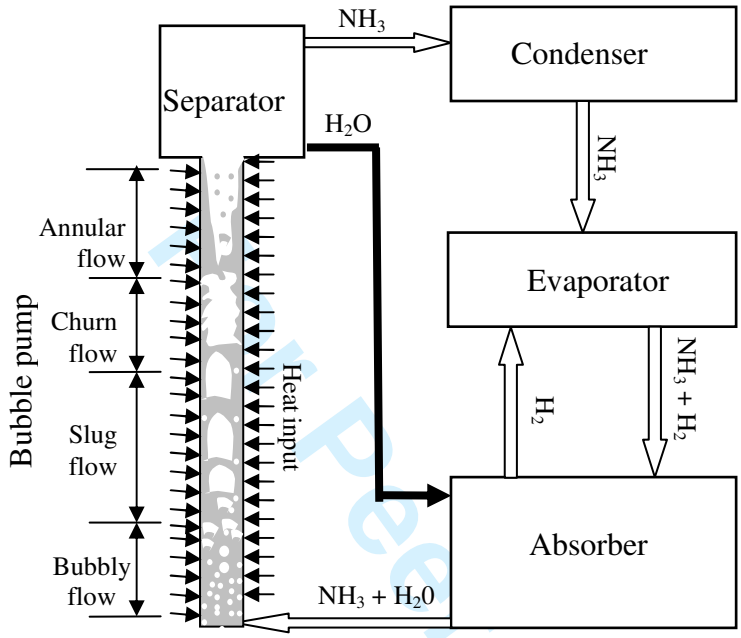

Fig. 1 Main components of an absorption-diffusion refrigeration cycle and flow configurations in the bubble pump

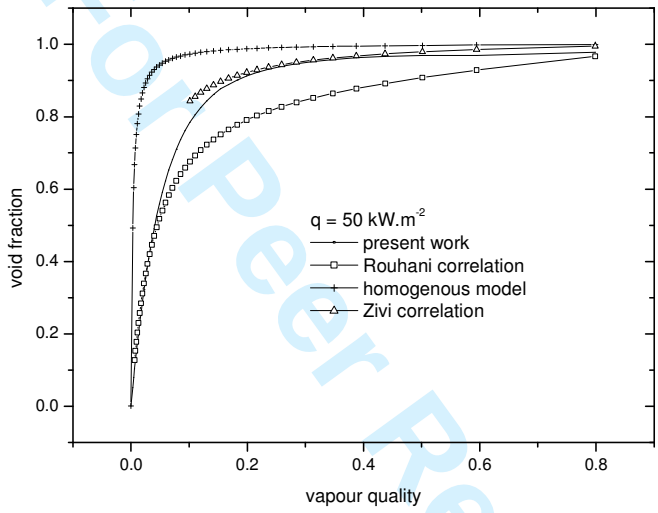

Fig. 2 Comparison of void fraction simulated with other models

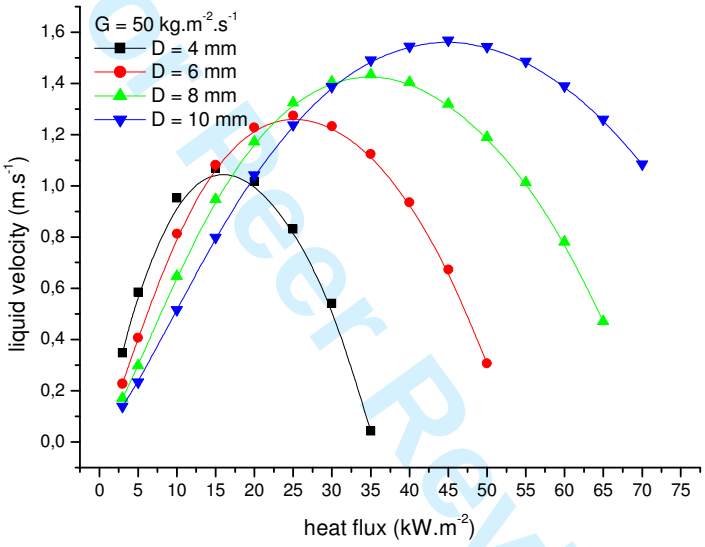

Fig. 3 Liquid velocity versus heat flux

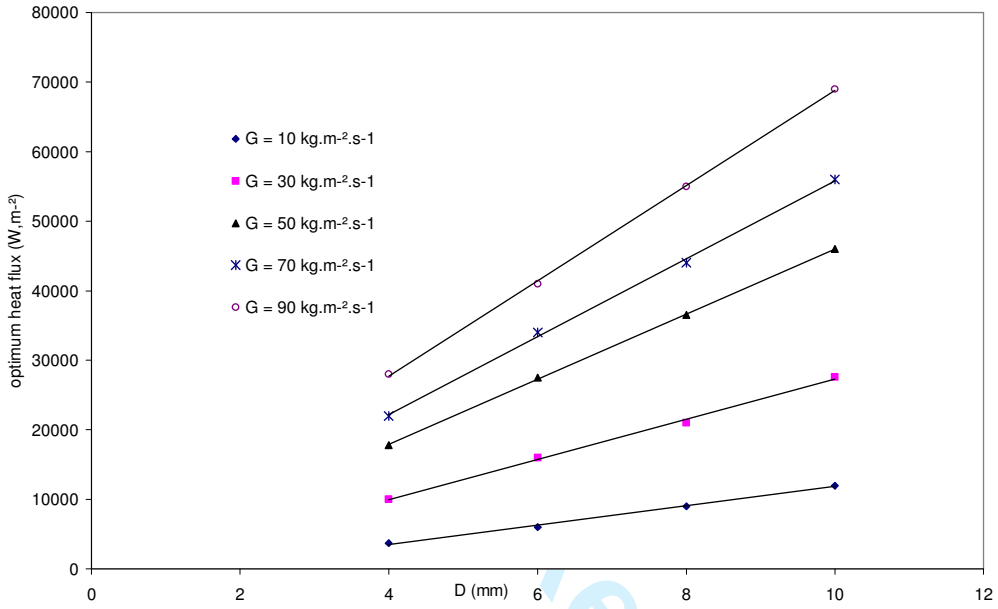

Fig. 4 Optimum heat flux versus tube diameter for different mass flow rates G

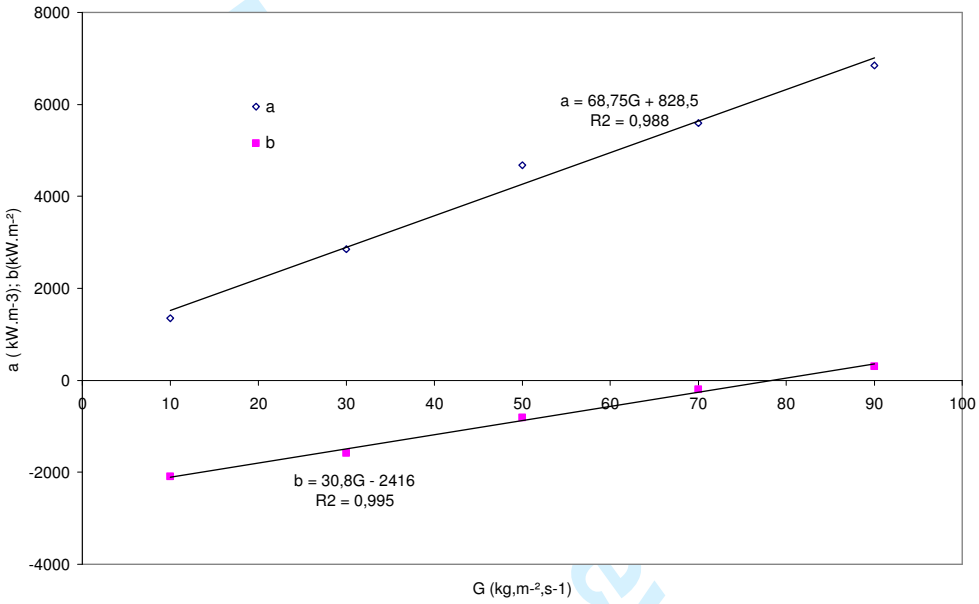

Fig. 5 Variations of parameters a and b versus the mass flow rate G

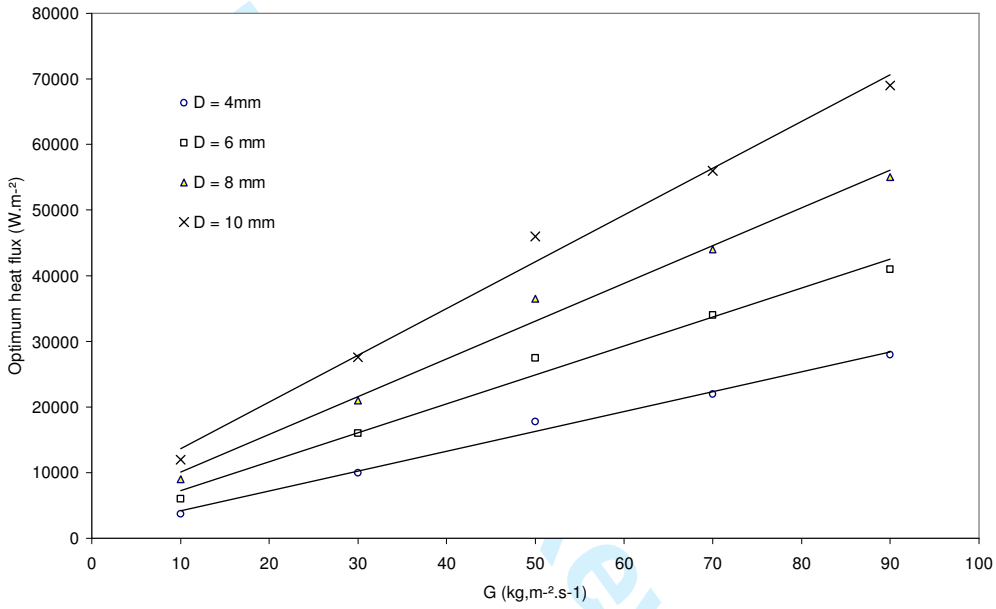

Fig. 6 Optimum heat flux versus mass flow rate for different tube diameter values

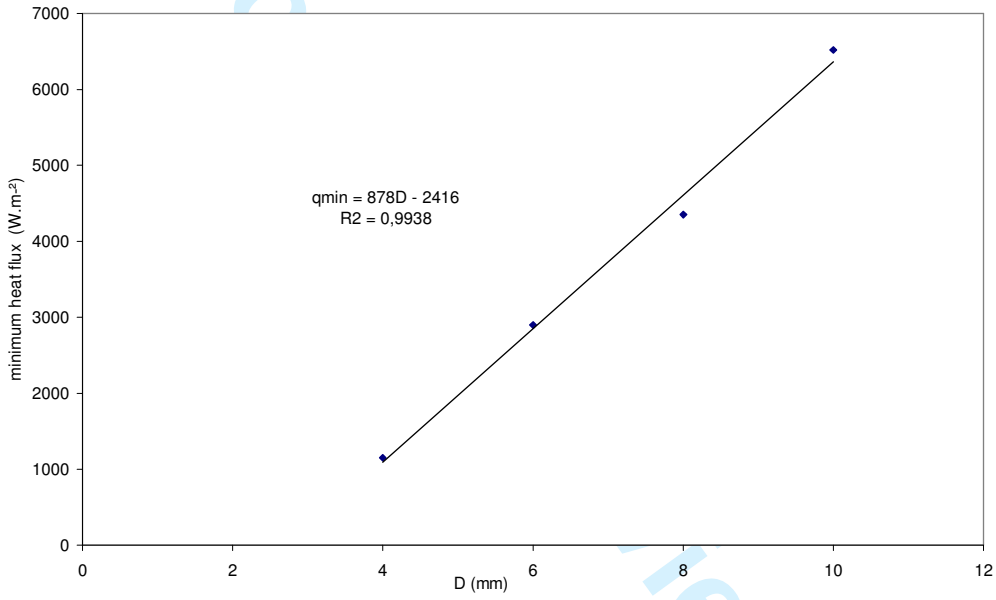

Fig. 7 Variations of minimum heat flux versus tube diameter D